SCIENTIFIC REPORTS

OPEN

Modulated scattering technique in the terahertz domain enabled by current actuated vanadium dioxide switches

Received: 21 July 2016
Accepted: 22 December 2016
Published: 01 February 2017

W. A. Vitale[1,*], M. Tamagnone[2,*], N. Émond[3], B. Le Drogoff[3], S. Capdevila[2], A. Skrivervik[2], M. Chaker[3], J. R. Mosig[2] & A. M. Ionescu[1]

The modulated scattering technique is based on the use of reconfigurable electromagnetic scatterers, structures able to scatter and modulate an impinging electromagnetic field in function of a control signal. The modulated scattering technique is used in a wide range of frequencies up to millimeter waves for various applications, such as field mapping of circuits or antennas, radio-frequency identification devices and imaging applications. However, its implementation in the terahertz domain remains challenging. Here, we describe the design and experimental demonstration of the modulated scattering technique at terahertz frequencies. We characterize a modulated scatterer consisting in a bowtie antenna loaded with a vanadium dioxide switch, actuated using a continuous current. The modulated scatterer behavior is demonstrated using a time domain terahertz spectroscopy setup and shows significant signal strength well above 0.5 THz, which makes this device a promising candidate for the development of fast and energy-efficient THz communication devices and imaging systems. Moreover, our experiments allowed us to verify the operation of a single micro-meter sized VO_2 switch at terahertz frequencies, thanks to the coupling provided by the antenna.

An electromagnetic scatterer is a structure able to scatter an impinging electromagnetic wave in various directions. Any object with electromagnetic properties different from the surrounding environment behaves as a scatterer. The modulated scattering technique (MST) is based on the modulation of the scattered field, which can be done by a mechanical change in the scatterer, or electronically using modulated scatterers (MS), which are linear passive electromagnetic devices able to control and change their electromagnetic scattering properties by embedding a tunable element[1].

The operating frequency of MS devices has been in the range of hundreds of kHz up to millimeter waves, while THz frequency range has not been explored yet. The terahertz domain, conventionally defined as the portion of the electromagnetic spectrum included between 0.3 THz and 3 THz, is currently a very active research topic for various applications, such as telecommunications, imaging, spectroscopy, radioastronomy and homeland security. However, a widespread diffusion of THz systems has been hindered by the relative lack of available devices to generate, manipulate and detect THz waves. Here we perform a step forward in this direction by proposing the first MS operating in the THz range.

Among other applications, MS have been extensively used for field mapping applications[1] and in radio frequency identification devices (RFID)[2,3], where the technique is used to encode information in the scattered signal by the device when interrogated with a single frequency harmonic impinging wave. This is achieved by time-modulation of the tunable element, which modulates the scattered field propagating away from the device. Recently, MS were also considered as an important alternative for phase far-field imaging applications[4,5]. As compared with classical imaging techniques based on bolometers, which are limited to amplitude information, MST allows measuring both the amplitude and the phase of an electromagnetic wave at a single point on the sensor.

[1]EPFL, Nanoelectronic Devices Laboratory (NanoLab), 1015 Lausanne, Switzerland. [2]EPFL, Laboratory of Electromagnetics and Antennas (LEMA), 1015 Lausanne, Switzerland. [3]INRS-Énergie, Matériaux et Télécommunications, 1650 Boulevard Lionel Boulet, Varennes, Québec J3X 1S2, Canada. *These authors contributed equally to this work. Correspondence and requests for materials should be addressed to W.A.V. (email: wolfgang.vitale@epfl.ch)

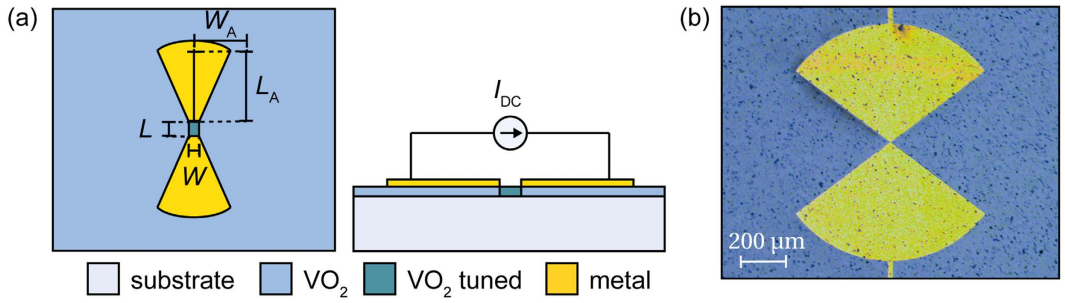

Figure 1. Structure of the proposed THz VO_2 modulated scatterer. (**a**) Schematic diagram and biasing circuit. The bowtie antenna is connected to a DC current generator used to actuate the VO_2 region in the antenna gap. (**b**) Top view of the fabricated device, with dimensions $L = 2\,\mu m$, $W = 4\,\mu m$, $L_A = 300\,\mu m$, $W_A = 400\,\mu m$, optimized to maximize the modulated signal.

This could be of great interest while considering an array of sensors, since having full knowledge of magnitude and phase for each pixel of the array would allow further processing not possible with only the knowledge of the received power (e.g. it could allow to re-focus the signal in a post-processing stage). Finally, single MS are very promising candidates for near-field imaging in the THz domain. Near-field imaging is already an extensively used technique at microwave frequencies[6,7] and our work opens the way to the implementation of this paradigm at THz frequencies. Moreover, since MST operates with a differential signal, this technique allows greater accuracy than fixed scatterer near-field imaging. The achievement of MST in the THz domain could thus lead to interesting new strategies to perform amplitude and phase imaging at THz frequencies. In this work, we explore the feasibility of a THz modulated scatterer using a wideband antenna and a vanadium dioxide (VO_2) switch as the tunable element (Fig. 1).

VO_2 is a strongly correlated material that undergoes a first-order phase transition from a low-temperature insulating state to a high-temperature metallic state when heated above its transition temperature (~340 K)[8]. This phase transition, which is accompanied by a structural change from monoclinic to tetragonal and a large variation of VO_2 electrical and optical properties[9], can also be triggered using electrical[10] or optical[11] excitations, which makes this material an excellent candidate for electronic and optical switching applications[12,13]. The VO_2 property exploited in this work is the steep reduction of its resistivity under electrical excitations. The proposed THz MS consists in a planar wideband bowtie metal antenna fabricated on a sapphire substrate, showing excellent transparency at THz frequencies, coated with a 500 nm VO_2 layer. The small gap in the center of the antenna ensures that when a DC current is applied along the two arms of the antenna, the VO_2 region in the antenna gap undergoes the phase transition and the scattering properties of the antenna are significantly altered due to the large decrease in the resistance of the switch. The exact nature of the physical mechanisms underlying the electrically-triggered metal-insulator transition in VO_2 is still under debate. However, it is generally agreed that the transition cannot rely solely on the thermal heating effect, as demonstrated by several works reporting switching times of the order of few nanoseconds[14–16].

It must be noticed that single VO_2 switches were not previously exploited for THz reconfigurable electronics. While such switches were already characterized for radiofrequency[17] and millimeter-wave[18] applications, the use of VO_2 in the THz range has been limited to the fabrication of metasurfaces in which the actuation of an unpatterned VO_2 film allows tuning the polarization[19,20], transmission[21,22] or resonance frequency[23,24] of the metasurface. The use of a single VO_2 switch in our device is crucial, as it ensures operation even when the interrogation field and the receiver are placed at arbitrary angles with respect to the modulated scatterer, which is not the case for metasurfaces, optimized to preserve the propagation direction of the modulated wave. Thanks to this property, the MS device proposed in this work enables new functionalities at THz frequencies, complementary to what is achievable with metasurfaces. Furthermore, the use of a single VO_2 switch reduces the power consumption and the response time of the device. Apart from modulation, it is worth mentioning that VO_2 has a promising technological potential for THz detection and generation applications, allowing the development of VO_2-based THz future front-end systems. For instance, THz generation from VO_2 has been achieved via optical non-linearities[25] or transient photocurrent contribution[26].

Results

Design and numerical simulations. The design procedure consists in optimizing the MS antenna and the VO_2 switch in order to maximize the power of the modulated signal P_{mod}. This is achieved by maximizing the difference in the scattered field in the two states of the MS. The MST theory is well known and demonstrates that the power of the modulated signal can be calculated using the modified Friis link budget equation[1]:

$$P_{mod} = P_T G_{TM} G_{MT} G_{MR} G_{RM} \left(\frac{\lambda}{4\pi}\right)^4 \frac{1}{R_{TM}^2 R_{RM}^2} \left|\Gamma_{ON}^K - \Gamma_{OFF}^K\right|^2 \quad (1)$$

where P_T is the power emitted by the transmitter, G_{TM} and G_{RM} are the gains of the transmitting and receiving antennas towards the MS respectively, G_{MT} and G_{MR} are the gains of the MS antenna towards the transmitting and receiving antennas respectively, R_{TM} and R_{RM} are the distances from the MS to the transmitting and receiving

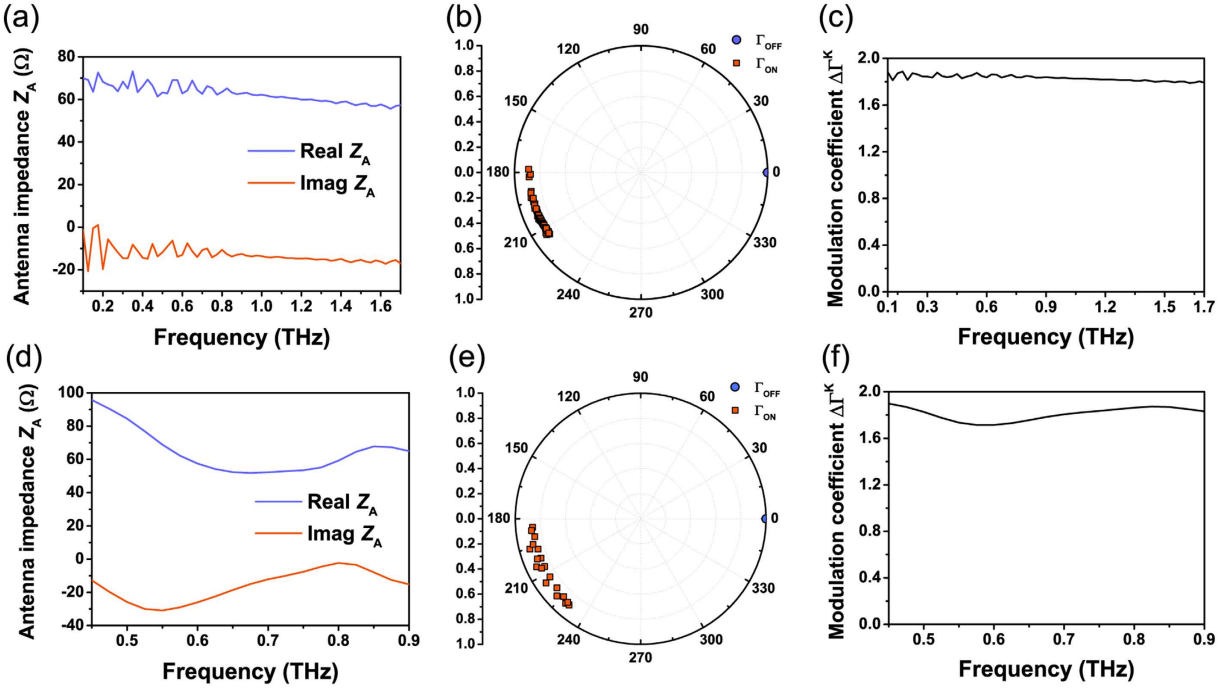

Figure 2. Simulations of THz modulated scatterers. (**a**) Input impedance Z_A for the antenna with optimized dimensions ($L_A = 300\,\mu m$, $W_A = 400\,\mu m$), simulated from 0.1 THz to 1.7 THz. (**b**) Reflection coefficient Γ^K for ON and OFF states for all the frequency points, obtained from the simulated Z_A values and the load impedance values for a VO_2 switch with length $L = 2\,\mu m$, width $W = 4\,\mu m$ and resistivities $\rho_{OFF} = 4.7 \cdot 10^{-1}\,\Omega\cdot m$, $\rho_{ON} = 4.3 \cdot 10^{-6}\,\Omega\cdot m$, extracted from four-point probe measurements of the VO_2 film used in this work. (**c**) Resulting modulation coefficient. (**d**) Input impedance Z_A for the antenna with reduced dimensions ($L_A = 60\,\mu m$, $W_A = 80\,\mu m$), simulated from 0.45 THz to 0.9 THz. (**e**) Reflection coefficient Γ^K for ON and OFF states for the smaller MS keeping the same VO_2 switch ($L = 2\,\mu m$, $W = 4\,\mu m$, $\rho_{OFF} = 4.7 \cdot 10^{-1}\,\Omega\cdot m$, $\rho_{ON} = 4.3 \cdot 10^{-6}\,\Omega\cdot m$). (**f**) Modulation coefficient for the smaller MS.

antennas respectively, λ is the wavelength and Γ^K is known as Kurokawa's reflection coefficient. Γ^K expresses the mismatch between the load and the antenna and it is defined as:

$$\Gamma^K_{ON} = \frac{Z_{ON} - Z_A^*}{Z_{ON} + Z_A};\ \Gamma^K_{OFF} = \frac{Z_{OFF} - Z_A^*}{Z_{OFF} + Z_A} \tag{2}$$

where Z_A is the input impedance of the MS antenna while Z_{ON} and Z_{OFF} are the impedances of the tunable load (here the VO_2 switch with length $L = 2\,\mu m$, width $W = 4\,\mu m$ and VO_2 thickness $t = 500\,nm$) in the ON and OFF states respectively.

Equation 1 shows that P_{mod} depends on the modulation coefficient $\Delta\Gamma^K$, defined as the difference of the reflection coefficients $\Delta\Gamma^K = |\Gamma^K_{ON} - \Gamma^K_{OFF}|$, which can be maximized by optimizing the antenna input impedance and the VO_2 switch impedance. Typical broadband bowtie antennas have input impedances with a constant real part (typically of the order of tens of ohms depending on both substrate and geometry) and a small imaginary part over the frequency band of interest. On the other hand, the VO_2 switch impedance is dominated by carrier dynamics in VO_2, which is approximately the same as in DC transport since the collision frequency is of the order of tens of terahertz[27–29], as confirmed by direct measurements of the THz conductivity showing negligible imaginary part and a real part with low dependence on frequency[30]. Hence, the VO_2 switch can be considered as resistive, i.e. its impedance is real, and its value can be computed from the bulk conductivity of VO_2 as $Z_{ON,OFF} = (\rho_{ON,OFF} L)/(Wt)$. Therefore, $\Delta\Gamma^K$ is maximized if $Z_A = Z_A^{OPT} \triangleq \sqrt{Z_{ON} Z_{OFF}}$[1]. Typical VO_2 switches have impedances of a few ohms in the ON state and of tens or even hundreds of kilohms in the OFF state, hence Z_A^{OPT} is expected to be of the order of kilohms. The antenna was thus optimized to maximize its input impedance while the switch was optimized to minimize Z_{ON}. For this reason a relatively large thickness $t = 500\,nm$ of VO_2 was used. Finally, using $\rho_{OFF} = 4.7 \cdot 10^{-1}\,\Omega\cdot m$ and $\rho_{ON} = 4.3 \cdot 10^{-6}\,\Omega\cdot m$ as obtained from four-point probe measurements, the load impedances are $Z_{OFF} = 4.7 \cdot 10^5\,\Omega$ and $Z_{ON} = 4.3\,\Omega$. The full resistivity dependence on temperature of the VO_2 film exploited in this work is reported in Supplementary Fig. S1.

The antenna optimization was performed by 3D electromagnetic simulations using Ansys HFSS and resulted in an impedance Z_A independent of frequency from 0.1 THz to 1.7 THz with low imaginary part (Fig. 2(a)) for an antenna with dimensions $L_A = 300\,\mu m$, $W_A = 400\,\mu m$. Introducing the values for Z_{ON} and Z_{OFF} previously obtained and the antenna impedance Z_A in Eq. (2), we obtain a high contrast between Γ^K_{ON} and Γ^K_{OFF} (Fig. 2(b)), resulting in a differential reflection coefficient $\Delta\Gamma^K \sim 1.8$ in the whole frequency range (Fig. 2(c)), which constitutes an excellent performance considering that the maximum possible value is 2. Moreover, the design can be scaled to

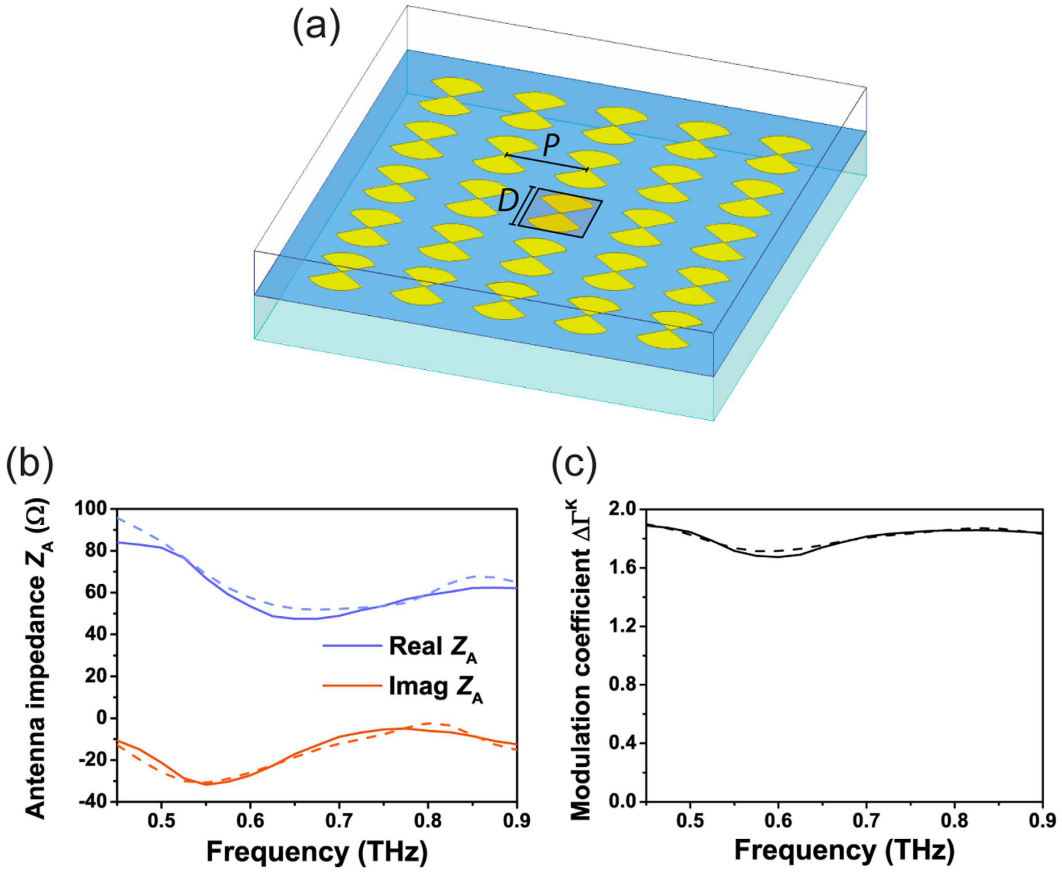

Figure 3. MS array simulations. (**a**) Full geometry domain for the electromagnetic simulation of an array of 5 × 5 MS ($L_A = 60\,\mu m$, $W_A = 80\,\mu m$, $D = 200\,\mu m$, $P = 250\,\mu m$), highlighting the MS for which the results are plotted in the following. (**b**) Antenna input impedance and (**c**) achieved modulation coefficient from 0.45 THz to 0.9 THz for the MS in the center of the array (solid lines) and an isolated MS with the same dimensions (dashed lines).

smaller dimensions while keeping the same W_A/L_A ratio, enabling the use of MS as a small near-field probe of circuits or antennas[1]. Figure 2(d–f) present the results of the simulations for a smaller antenna in a range of THz frequencies such that $0.3 < D/\lambda < 0.6$, where λ is the wavelength and D is the diameter of the smallest circumference that can circumscribe the antenna. This condition is satisfied from 0.45 THz to 0.9 THz for an antenna with $W_A = 80\,\mu m$, $L_A = 60\,\mu m$, resulting in $D = 200\,\mu m$. As shown in Fig. 2(d), even in the case of an electrically small antenna, the bowtie design allows to achieve an impedance with a low imaginary part and a real part presenting low dependence on frequency, allowing to achieve a high difference in reflection coefficients ($\Delta\Gamma^K > 1.7$, Fig. 2(f)) and, as a consequence, to maximize the power of the modulated signal. If further antenna miniaturization is required for any targeted application, the antenna can be modified using well known miniaturized antenna designs; however the improvement in miniaturization implies either a reduction in bandwidth or an increase in the losses of the antenna, in accordance with the Chu-Harrington limit[31].

Further simulations were performed to address the feasibility of imaging applications based on the MST. Complex imaging involves heavy processing of the near-field information (magnitude and phase) in a given area of space, which can be provided with the use of MS arrays that would sample the field at the different positions of each MS probe. For this reason, we used the small MS sensor ($D = 200\,\mu m$) to simulate an array of 5 × 5 MS, as shown in Fig. 3(a). The pitch $P = 250\,\mu m$ between the centers of the antennas is selected in order to have $P/\lambda = 0.5$ and $D/\lambda = 0.4$ for a frequency $f_0 = 0.6$ THz. As shown in Fig. 3(b), the presence of additional sensors is not altering significantly their broadband performance as compared to a single antenna. As a consequence, $\Delta\Gamma^K$ is still higher than 1.65 in the whole frequency range of interest (Fig. 3(c)), demonstrating that the use of the proposed MST with a VO_2 junction can be extended to an array without altering its design.

Measurements. The fabricated MS with optimized dimensions ($L = 2\,\mu m$, $W = 4\,\mu m$, $L_A = 300\,\mu m$, $W_A = 400\,\mu m$) was first measured in DC in order to characterize the electrical actuation of the VO_2 switch integrated in the THz antenna. All the measurements were performed at room temperature. Figure 4(a) shows the resistance modulation of the VO_2 switch due to the increase in direct current up to 20 mA. The measured resistance in the OFF state is 1.25 kΩ, which is considerably lower than that used in the design due to the current leakage flowing in the VO_2 material outside the antenna gap: the parasitic resistance between the bias lines is in parallel to the modulated VO_2 resistance inside the gap, decreasing the measured Z_{OFF} value. However, the

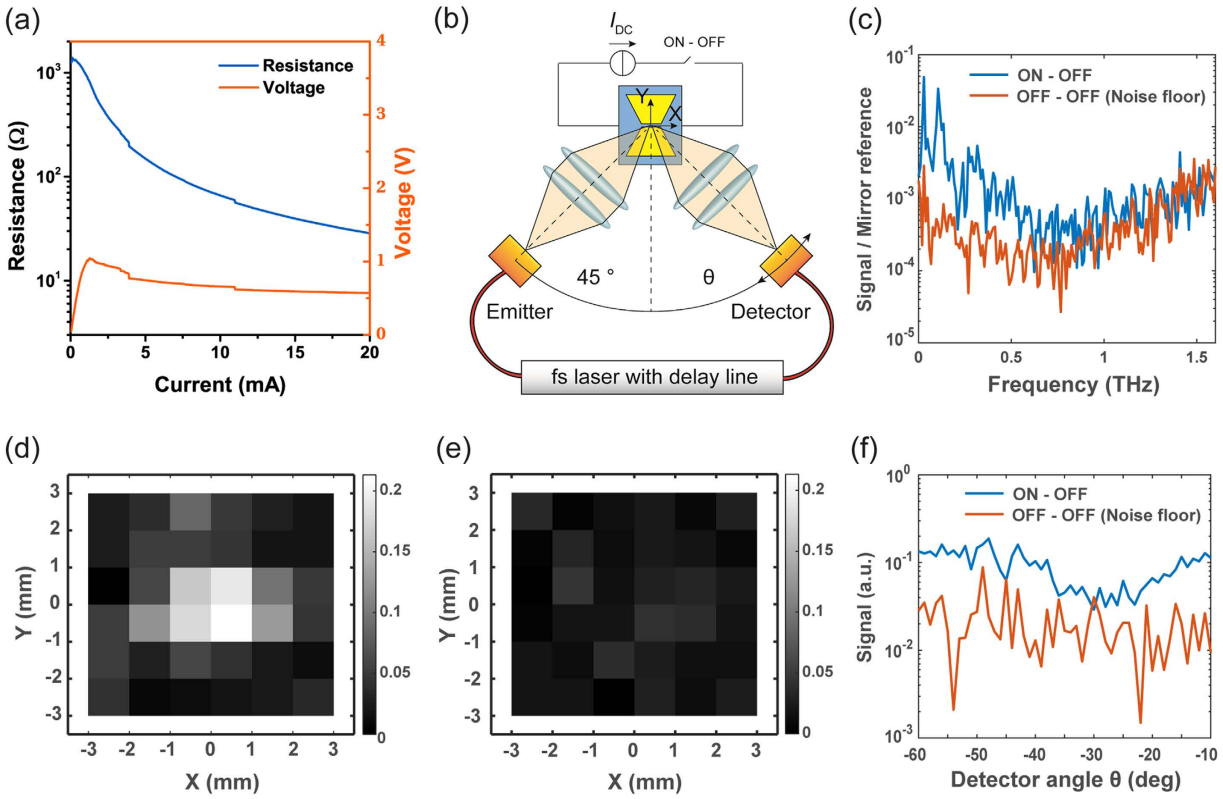

Figure 4. MS characterization. (**a**) DC characterization of the VO_2 switch. (**b**) Schematic diagram of the THz measurement setup, including the rotary stage for the detector arm at angle θ, the imaging stage to move the MS in the XY plane and the DC biasing scheme with direct current $I_{DC} = 20$ mA. (**c**) THz differential signal normalized to the mirror reference with 10^3 measurements cycles averaging and the receiving detector at −10°. (**d**) Differential signal and (**e**) noise floor imaging at 0.32 THz with 10^2 cycles averaging while the setup is focused on the center (X = 0 mm, Y = 0 mm) and the MS is moved in a 6×6 mm^2 area around the center. (**f**) Scattering pattern at 0.32 THz with 10^2 cycles averaging.

performance of the THz MS is not affected, as it solely depends on the modulation of the impedance of the region inside the gap. The measured Z_{OFF} value thus represents a pessimistic estimate for the Z_{OFF} design parameter used in eq. (2) to calculate Γ^K_{OFF}. The resistance in the ON state depends on the bias current and it is 149 Ω at 5 mA and 28.5 Ω at 20 mA. In order to limit the power consumption and prevent reliability issues, the current was limited to 20 mA while operating the device, which was not high enough to reach the Z_{ON} value used in the design, but still low enough to ensure a good modulation coefficient (see Supplementary Fig. S2). The measured Z_{ON} value includes the finite contact resistance between VO_2 and gold (Au) metal contacts[16,32], whose effect is reduced at THz frequencies due to the parasitic contact capacitance in parallel.

Next, the operation of the device as a MS was proven using a fiber coupled time-domain THz spectroscopy system (Menlo TERA K15) in the configuration represented in Fig. 4(b). The transmission arm, which includes the THz emitter and a focusing lens, is placed at 45 degrees with respect to the sample normal, while the receiver arm, which includes another focusing lens and the detector, is mounted on a rotary stage at an angle θ with respect to the normal, allowing to perform scattering pattern measurements. The arm lenses lie at focal distance from the antenna to improve the signal-to-noise ratio (SNR) and the polarization of the THz beam is aligned to the polarization of the antenna (vertical polarization). The sample is glued and wire-bonded to a printed circuit board and mounted on XY imaging stages. All the measurements were performed at room temperature. The differential signal is obtained by subtracting the received field when the VO_2 switch is in the OFF state from the one measured when the switch is ON ($I_{DC} = 20$ mA). The reference noise floor is obtained by measuring a second time the MS in the OFF state and subtracting it from the previous OFF state. All the measurements are normalized to the power of the THz pulse, obtained by measuring the received signal reflected by a mirror. The measurements were repeated for several cycles and averaged.

Figure 4(c) shows the received differential signal averaged for 1000 cycles as a function of frequency. The differential signal is well above the noise floor in the THz range and the maximum operation frequency is larger than 0.5 THz (see Supplementary Fig. S3 for the error bounds on the average signal). The decrease in performance with frequency is expected because of the imperfect focusing of the THz system, which limits the electromagnetic power coupled to the VO_2 switch at high frequency. Some important considerations can be made on the unusual noise floor signal in Fig. 4(c). This signal is actually the difference of two quantities whose values are expected to be identical and, therefore, it represents both the random and the systematic errors. However, because the signal is normalized to the mirror reference, its shape is not monotonic and it instead represents the inverse of the SNR of

our measurement setup, which is maximal at approximately 0.6 THz and decreases for higher and lower frequencies. Figure 4(d) shows an image of the differential signal averaged over 100 cycles obtained by moving the sample in the XY plane with the imaging stage (the noise floor is shown in Fig. 4(e) for comparison). The measurements were performed at 0.32 THz, where we observed the maximum SNR. This image demonstrates that the source of the differential signal is indeed localized on the MS and not due to other effects, since we observe a signal above the noise floor only when the MS is aligned to the focus. Finally, the measured radiation pattern of the MS at 0.32 THz, obtained for different angles of the receiving arm (the transmission arm being kept at 45° from the normal) is shown in Fig. 4(f), indicating that operation is possible over a wide range of angles.

Discussion

We demonstrated the modulated scatterer technique in the THz domain and used VO_2 as a tunable material to enable device operation on a wide range of frequencies well above 0.5 THz. We were also able to verify the operation of a single μm-sized VO_2 switch in the THz range due to the excellent coupling with the antenna. These achievements were made possible by efficiently exploiting the large and steep decrease of the VO_2 switch resistivity across the metal-insulator transition, which enables the scattering properties of the antenna to be altered. Furthermore, the MS structure scatters the incident THz wave in a wide range of directions, which allows different applications with respect to standard VO_2 metasurfaces. This device is thus a very promising candidate for the development of fast and energy-efficient THz communication applications and phase-resolved THz imaging systems.

Methods

VO_2 deposition. A VO_2 thin film of 500 nm thickness was grown on *r*-cut oriented sapphire substrates (Al_2O_3 ($1\bar{1}02$)) by reactive pulsed laser deposition (RPLD) using a KrF laser ($\lambda = 248$ nm) at a repetition rate of 10 Hz. The vanadium metal target was ablated at a fluence of 2 J/cm^2. Prior to deposition, the chamber was pumped down to 10^{-6} Torr. During deposition, the oxygen pressure was kept at 27 mTorr with a constant oxygen flow of 5 sccm. The target-to-substrate distance was set at 6.5 cm and the substrate temperature was maintained at 550 °C. Detailed growth conditions have been reported in a previous study[33]. The film thickness was determined by cross-section scanning electron microscopy (SEM) observations.

MS fabrication. The THz bowtie antenna was fabricated on the top of the VO_2 film by means of electron beam lithography (EBL). A 1 μm thick layer of poly(methyl-methacrylate) (PMMA) 950 K A7 from Microchem was first spin-coated on top of the VO_2 film and baked at 180 °C for 5 minutes. The EBL was then performed at 100 keV and 60 nA using a VB6 UHR EWF (Raith Inc.), followed by the development of the exposed sample in a solution of methyl-isobutyl-ketone (MIBK) (1 vol.) and isopropyl alcohol (IPA) (3 vol.) for 75 s. Deposition of a 100 nm thick metal layer (90 nm Au)/(10 nm Cr) was performed after development by means of electron beam evaporation (K.J. Lesker AXXIS). The resist was then removed in dichloromethane and the sample was rinsed in acetone and IPA before being blown dry with pure nitrogen gas.

Numerical simulations. The MS antennas were optimized by 3D full-wave electromagnetic simulations in the THz range, performed using the commercial simulation package Ansys HFSS. The boundaries of the simulation domain are at a distance from the antenna of at least $\lambda_g/4$ in all directions, where λ_g is the wavelength in the medium, calculated at the minimum simulated frequency. The simulation was performed applying a lumped port in the gap between the two arms of the antenna. Radiation boundary conditions are applied to all the outer faces of the simulation domain. The relative permittivity of the sapphire substrate is $\varepsilon_{sap} = 10$ and the VO_2 layer was assumed to have a relative permittivity in the insulating state $\varepsilon_{VO2} = 30$. Gold was simulated as a lossy conductor with conductivity $\sigma_{Au} = 4.1 \times 10^7$ S/m.

References

1. Bolomey, J.-C. & Gardiol, F. *Engineering Applications of the Modulated Scatterer Technique*. (Artech House, 2001).
2. Bolomey, J. C., Capdevila, S., Jofre, L. & Romeu, J. Electromagnetic Modeling of RFID-Modulated Scattering Mechanism. Application to Tag Performance Evaluation. *Proc. IEEE* **98,** 1555–1569 (2010).
3. Capdevila, S., Jofre, L., Bolomey, J.-C. & Romeu, J. RFID Multiprobe Impedance-Based Sensors. *IEEE Trans. Instrum. Meas.* **59,** 3093–3101 (2010).
4. Abou-Khousa, M. & Zoughi, R. Multiple Loaded Scatterer Method for E-Field Mapping Applications. *IEEE Trans. Antennas Propag.* **58,** 900–907 (2010).
5. Ghasr, M. T., Abou-Khousa, M. a., Kharkovsky, S., Zoughi, R. & Pommerenke, D. Portable Real-Time Microwave Camera at 24 GHz. *IEEE Trans. Antennas Propag.* **60,** 1114–1125 (2012).
6. Dyson, J. D. Measurement of Near Fields of Antennas and Scatterers. *IEEE Trans. Antennas Propag.* **21,** 446–460 (1973).
7. Memarzadeh Tehran, H., Laflamme-Mayer, N., Laurin, J. J. & Kashyap, R. A near-field measurement setup using an array of optically modulated scatterers. in *Conference Proceedings of the International Symposium on Signals, Systems and Electronics* 481–484, doi: 10.1109/ISSSE.2007.4294518 (2007).
8. Morin, F. J. Oxides which show a metal-to-insulator transition at the neel temperature. *Phys. Rev. Lett.* **3,** 34–36 (1959).
9. Verleur, H. W., Barker, A. S. & Berglund, C. N. Optical properties of VO_2 between 0.25 and 5 eV. *Rev. Mod. Phys.* **40,** 737 (1968).
10. Ruzmetov, D., Gopalakrishnan, G., Deng, J., Narayanamurti, V. & Ramanathan, S. Electrical triggering of metal-insulator transition in nanoscale vanadium oxide junctions. *J. Appl. Phys.* **106** (2009).
11. Cavalleri, A., Dekorsy, T., Chong, H. H. W., Kieffer, J. C. & Schoenlein, R. W. Evidence for a structurally-driven insulator-to-metal transition in VO_2: A view from the ultrafast timescale. *Phys. Rev. B - Condens. Matter Mater. Phys.* **70,** 1–4 (2004).
12. Zheludev, N. I. & Kivshar, Y. S. From metamaterials to metadevices. *Nat. Mater.* **11,** 917–924 (2012).
13. Yang, Z., Ko, C. & Ramanathan, S. Oxide Electronics Utilizing Ultrafast Metal-Insulator Transitions. *Annu. Rev. Mater. Res.* **41,** 337–367 (2011).
14. Leroy, J. *et al.* High-speed metal-insulator transition in vanadium dioxide films induced by an electrical pulsed voltage over nanogap electrodes. *Appl. Phys. Lett.* **100,** 213507 (2012).

15. Zhou, Y. *et al.* Voltage-Triggered Ultrafast Phase Transition in Vanadium Dioxide Switches. *IEEE Electron Device Lett.* **34,** 220–222 (2013).
16. Joushaghani, A. *et al.* Electronic and thermal effects in the insulator-metal phase transition in VO2 nano-gap junctions. *Appl. Phys. Lett.* **105,** 231904 (2014).
17. Vitale, W. A. *et al.* Steep slope VO_2 switches for wide-band (DC-40 GHz) reconfigurable electronics. in *72nd Device Research Conference* 29–30, doi:10.1109/DRC.2014.6872284 (2014).
18. Hillman, C., Stupar, P. A. & Griffith, Z. VO_2 Switches for Millimeter and Submillimeter-Wave Applications. In *2015 IEEE Compound Semiconductor Integrated Circuit Symposium* (*CSICS*) 1–4, doi: 10.1109/CSICS.2015.7314528 (IEEE, 2015).
19. Vegesna, S. *et al.* Terahertz frequency selective surface with reconfigurable polarization characteristics using vanadium dioxide. *J. Electromagn. Waves Appl.* **28,** 83–90 (2014).
20. Shin, J.-H., Moon, K., Lee, E. S., Lee, I.-M. & Hyun Park, K. Metal-VO_2 hybrid grating structure for a terahertz active switchable linear polarizer. *Nanotechnology* **26,** 315203 (2015).
21. Jeong, Y.-G. *et al.* Electrical control of terahertz nano antennas on VO_2 thin film. *Opt. Express* **19,** 21211–5 (2011).
22. Jeong, Y.-G. *et al.* A Vanadium Dioxide Metamaterial Disengaged from Insulator-to-Metal Transition. *Nano Lett.* **15,** 6318–6323 (2015).
23. Driscoll, T. *et al.* Dynamic tuning of an infrared hybrid-metamaterial resonance using vanadium dioxide. *Appl. Phys. Lett.* **93,** 24101 (2008).
24. Zhu, Y. *et al.* Tunable dual-band terahertz metamaterial bandpass filters. *Opt. Lett.* **38,** 2382–4 (2013).
25. Esaulkov, M. *et al.* Emission of terahertz pulses from vanadium dioxide films undergoing metal–insulator phase transition. *Optica* **2,** 790 (2015).
26. Charipar, N. A., Kim, H., Mathews, S. A. & Piqué, A. Broadband terahertz generation using the semiconductor-metal transition in VO_2. *AIP Adv.* **6,** 15113 (2016).
27. Wang, H., Yang, Y. & Wang, L. Wavelength-tunable infrared metamaterial by tailoring magnetic resonance condition with VO_2 phase transition. *J. Appl. Phys.* **116,** 123503 (2014).
28. Hilton, D. J. *et al.* Enhanced Photosusceptibility near T_c for the Light-Induced Insulator-to-Metal Phase Transition in Vanadium Dioxide. *Phys. Rev. Lett.* **99,** 226401 (2007).
29. Peterseim, T., Dressel, M., Dietrich, M. & Polity, A. Optical properties of VO_2 films at the phase transition: Influence of substrate and electronic correlations. *J. Appl. Phys.* **120,** 75102 (2016).
30. Cocker, T. L. *et al.* Terahertz conductivity of the metal-insulator transition in a nanogranular VO_2 film. *Appl. Phys. Lett.* **97,** 19–22 (2010).
31. Chu, L. J. Physical Limitations of Omni-Directional Antennas. *J. Appl. Phys.* **19,** 1163 (1948).
32. Joushaghani, A. *et al.* Voltage-controlled switching and thermal effects in VO2 nano-gap junctions. *Appl. Phys. Lett.* **104,** 221904 (2014).
33. Émond, N., Hendaoui, A. & Chaker, M. Low resistivity $W_xV_{1-x}O_2$-based multilayer structure with high temperature coefficient of resistance for microbolometer applications. *Appl. Phys. Lett.* **107,** 143507 (2015).

Acknowledgements

The authors are grateful to Thales Group, to Hasler Foundation (Project 11149), to the Swiss National Science Foundation (SNSF grant 133583), to the Canada Research Chair program and to the "Fonds de recherche du Quebec—Nature et technologies (FRQNT)" for their financial support.

Author Contributions

M.T. conceived the idea of the terahertz modulated scatterer based on vanadium dioxide. W.A.V. designed the final structures and carried out the electromagnetic simulations. N.E. and B.Le D. designed the process flow and fabricated the device. M.T. and S.C. designed and performed the measurements in the time domain terahertz spectroscopy setup and processed the data. W.A.V., M.T., S.C. and N.E. wrote the article. A.S., M.C., J.R.M. and A.M.I. discussed the results and commented on the manuscript. A.M.I. directed the overall project.

Additional Information

Supplementary information accompanies this paper at http://www.nature.com/srep

Competing financial interests: The authors declare no competing financial interests.

How to cite this article: Vitale, W. A. *et al.* Modulated scattering technique in the terahertz domain enabled by current actuated vanadium dioxide switches. *Sci. Rep.* **7**, 41546; doi: 10.1038/srep41546 (2017).

Publisher's note: Springer Nature remains neutral with regard to jurisdictional claims in published maps and institutional affiliations.